Research Article
Vol. 21, No. 6, Jan.-Feb. 2026, p.

Effects of Cold Plasma and Nano-zinc Oxide on Modification of Corn Starch as a Food Packaging Material

A.H. Bayanloo[1], I. Shahabi-Ghahfarrokhi[1,2*], S. Hagh-Nazari[1]

1- Department of Food Science and Engineering, Faculty of Agriculture, University of Zanjan, Zanjan, Iran
2- Department of Food Science and Technology, College of Agriculture, Isfahan University of Technology, Isfahan Iran
(*- Corresponding Author Email: i.shahabi@znu.ac.ir)

Received:	17.07.2025
Revised:	02.09.2025
Accepted:	21.09.2025
Available Online:	02.12.2025

How to cite this article:
Bayanloo, A.H., Shahabi-Ghahfarrokhi, I., & Hagh-Nazari, S. (2026). Effects of cold plasma and nano-zinc oxide on modification of corn starch as a food packaging material. *Iranian Food Science and Technology Research Journal, 21*(6),. https://doi.org/10.22067/ifstrj.2025.94463.1455

Abstract

This study explores the effects of cold plasma (CP) treatment on eco-friendly starch/ZnO (SZ) bio-nanocomposite films, incorporating 3 wt% nano-ZnO (ZnO NPs) and varying CP exposure times (0, 30, 60, 90 s). The results indicate that prolonged CP treatment increases film thickness, viscosity, water solubility, moisture absorption, and surface roughness, while reducing contact angle and moisture content. No significant changes were observed in water vapor permeability, density, or UV-Vis properties. CP treatment enhanced tensile strength, elongation at break, and tensile energy to break, while decreasing lightness and whiteness indices without altering color difference. The study highlights CP as a rapid, eco-friendly method for modifying films, with greater efficacy when applied to aqueous starch solutions, offering potential for industrial-scale applications in packaging materials.

Keywords: Cold plasma, Dual-modification, Green packaging, Nanocomposite, Starch, ZnO

Introduction

Packaging serves a vital function in preserving the integrity of food products, prolonging their shelf life, conveying essential information to consumers, and ensuring efficient distribution and transportation. These roles underscore its significance in maintaining food quality, safety, and accessibility throughout the supply chain (Venkateshaiah *et al.*, 2021). However, the widespread reliance on petroleum-derived plastics in the packaging sector has resulted in persistent environmental contamination, as these materials are neither biodegradable nor compostable. This has significantly contributed to the accumulation of non-degradable waste, posing serious ecological challenges (Cheng *et al.*, 2021). To address this issue, researchers have been focusing on developing biodegradable alternatives, with starch being considered one of the most promising biopolymers due to its abundance, availability, cost-effectiveness, and film-forming properties (Shahabi-Ghahfarrokhi, Almasi, & Babaei-Ghazvini, 2020).

Despite its advantages, starch-based packaging materials have limitations such as high sensitivity to moisture, excessive water vapor permeability (WVP), and poor mechanical properties (Babaei-Ghazvini, Shahabi-Ghahfarrokhi, & Goudarzi, 2018; Goudarzi, Shahabi-Ghahfarrokhi, & Babaei-Ghazvini, 2017). To overcome these drawbacks, various approaches have been explored, including incorporation with other

https://doi.org/10.22067/ifstrj.2025.94463.1455

biopolymers (Goudarzi & Shahabi-Ghahfarrokhi, 2018a), chemical modification (Wihodo & Moraru, 2013), the use of different plasticizers (Almasi, Ghanbarzadeh, & Entezami, 2010), nanocomposite formation (Goudarzi & Shahabi-Ghahfarrokhi, 2018a; Goudarzi *et al.*, 2017; Shahabi-Ghahfarrokhi & Babaei-Ghazvini, 2019), UV irradiation (Goudarzi & Shahabi-Ghahfarrokhi, 2018b; Shahabi-Ghahfarrokhi, Goudarzi, & Babaei-Ghazvini, 2019), and γ-irradiation (Ali & Ghaffar, 2017). Among these strategies, the integration of nanoparticles into the biopolymer matrix has demonstrated significant potential in enhancing the functional properties of starch-based nanocomposites. Achieving optimal performance relies heavily on the uniform dispersion of nanoparticles within the matrix, as the aggregation of nanoparticles can compromise the overall efficiency and effectiveness of the nanocomposites (Babaei-Ghazvini *et al.*, 2018; Goudarzi & Shahabi-Ghahfarrokhi, 2018a, 2018b; Salarbashi *et al.*, 2016; Shahabi-Ghahfarrokhi & Babaei-Ghazvini, 2019; Shahabi-Ghahfarrokhi, Khodaiyan, Mousavi, & Yousefi, 2015b). Moreover, nanocomposites with antimicrobial properties (Salarbashi *et al.*, 2016) and UV-barrier properties (Babaei-Ghazvini *et al.*, 2018; Goudarzi *et al.*, 2017; Shahabi-Ghahfarrokhi *et al.*, 2015b) have emerged as active packaging technology.

ZnO NPs offers several desirable properties, including photoactivity, antimicrobial activity, cost-effectiveness, non-toxicity, UV protection, and biocompatibility, making it suitable for active food packaging applications (Babaei-Ghazvini *et al.*, 2018; El Fawal *et al.*, 2020; Liu et al., 2021; Salarbashi *et al.*, 2016; Shahabi-Ghahfarrokhi & Babaei-Ghazvini, 2019; Shahabi-Ghahfarrokhi *et al.*, 2015b). The nutritional quality, flavor, and safety of food can be compromised by UV radiation through the process of lipid oxidation, which results in the development of toxic compounds. By using UV-protective food packaging materials, the need for synthetic antioxidants can be reduced (Shahabi-Ghahfarrokhi *et al.*, 2015b).

However, the migration of nanoparticles into food and the potential ingestion of these nano compounds raise concerns. To minimize the risk, researchers have proposed enhancing the compatibility between the nanoparticles and the polymer matrix (Souza & Fernando, 2016). A previous study used UV rays to improve the compatibility of ZnO NPs in a bio nanocomposite (Shahabi-Ghahfarrokhi & Babaei-Ghazvini, 2019); however, this process is time-consuming and unsuitable for industrial-scale production.

Plasma, characterized as a quasi-neutral ionized gas and recognized as the fourth state of matter, has gained prominence as an environmentally sustainable technology with diverse applications. These include food sanitization, biomedical advancements, semiconductor manufacturing, and innovative packaging solutions (Dimitrakellis & Gogolides, 2018). Plasma exists as hot and CP. Thermal plasma is a state of plasma in which all constituent species—electrons, ions, and neutrals—exist in a condition of local thermodynamic equilibrium, resulting in a single, uniform temperature that can exceed 10,000 K. In contrast, non-thermal plasma, often referred to as CP, is characterized by a significant thermodynamic non-equilibrium state. In this state, electrons possess a very high temperature (energy), while heavy particles, such as ions and neutral species, remain close to ambient temperature (Sharma, 2020). CP is a particularly promising technique due to its cost-effectiveness, non-thermal nature, ease of access, and environmental friendliness. CP can be used to modify biopolymers and improve their properties, such as adhesion and printability (Heidemann, Dotto, Laurindo, Carciofi, & Costa, 2019). Key factors that influence the CP process include treatment duration, feed gas, electric field strength, and the applied electrical power (Maniglia, Castanha, Rojas, & Augusto, 2021). Although CP has been utilized in prior study to modify starch-based films, the process has been reported to be time-intensive (Goiana *et al.*, 2021), often requiring treatment times ranging from 10 to 20 min. Therefore, for industrial applications,

a rapid and efficient CP procedure is necessary.

This study employed CP as a rapid (<90 s) and environmentally benign treatment to modify starch-based films, thereby improving the compatibility of ZnO NPs with the biopolymer matrix. The resulting modified SZ bionanocomposite was investigated as a food packaging material. This approach provides a promising pathway for the design and production of eco-friendly packaging materials with enhanced performance characteristics.

Materials and Methods

Materials

Corn starch, was sourced from Zarrin Corn Company (Shahroud, Iran). ZnO NPs with average size of 30–40 nm was acquired from Tecnan (Spain). High-purity analytical grade reagents were procured from commercial suppliers as follows: magnesium nitrite and glycerol were obtained from Merck KGaA (Darmstadt, Germany), while sodium chloride and calcium chloride were sourced from Dr. Mojalali Co. (Tehran, Iran).

Film Preparation

A 5% (wt%) starch solution was prepared in distilled water (DW) and heated to 80°C while stirring continuously for 30 min using a heater magnetic stirrer. Glycerol, added at 45% of the dry weight, was incorporated as a plasticizer and stirred for an additional 10 min to improve the flexibility of the films. A suspension of ZnO NPs was prepared in DW at a final concentration of 3% (w/w, dry basis). The suspension was stirred for 10 min and subsequently sonicated for 30 min in an ultrasonic bath (vCLEAN1 – L2, Viera Tejarat Backer Co, Iran). This ZnO NP suspension was then introduced gradually into the film-forming solution under continuous stirring for 10 min. The resulting mixture was placed 2.5 cm from the nozzle of a jet CP system (Plasmatech-18A, Super arc plasma, Iran). Using air as the feed gas at a power output of 2100 W, the solution was subjected to plasma irradiation (Fig. 1) while being agitated continuously with a magnetic stirrer to ensure homogeneity. Following exposure to CP for 30, 60, and 90 s, the film-forming solutions were cast onto level, non-sticking polystyrene plates (15 cm diameter) and dried for 48 h at ambient temperature. The resulting films were subsequently peeled from the casting surface. Prior to analysis, all samples were conditioned for 48 h at 50–55% relative humidity (RH).

Fig. 1. The experimental setup for the cold plasma irradiation of starch/ZnO NPs film-forming solutions using a jet cold plasma system

Physical Characteristics

Microstructure

The surface and cross-sectional morphology of the film specimens, along with the dispersion of ZnO NPs, were characterized using a field emission scanning electron microscope (FE-SEM; TESCAN MIRA3, Czech Republic). To prepare cross-sectional views, the films were cryogenically fractured in liquid nitrogen. All samples were mounted on aluminum stubs with double-sided carbon tape and sputter-coated with a thin layer of gold to ensure electrical conductivity prior to imaging.

Intrinsic Viscosity

The intrinsic viscosity, [η], of the samples was determined by extrapolating the reduced and inherent viscosity to infinite dilution using the Huggins (Eq. 1) and Kraemer (Eq. 2) equations (Ghasemlou, Khodaiyan, Jahanbin, Gharibzahedi, & Taheri, 2012; Goudarzi & Shahabi-Ghahfarrokhi, 2018b). Intrinsic viscosity was measured in triplicate.

$$\frac{\eta_{sp}}{C} = [\eta] + k_H [\eta]^2 C \quad (1)$$

$$\frac{\ln(\eta_{rel})}{C} = [\eta] + k_k [\eta]^2 C \quad (2)$$

The intrinsic viscosity ([η]), specific viscosity (η_{sp}), and relative viscosity (η_rel) are fundamental parameters in this analysis. The values of η_{sp} and η_{rel} were calculated using Eq. (3) and (4), respectively. The Huggins (K_H) and Kraemer (K_K) coefficients, alongside the polymer concentration (C), are key constants in the respective models. Measurements of intrinsic viscosity were conducted at a constant temperature of 24 °C using a Cannon-Fenske routine capillary viscometer.

$$\eta_{rel} = \frac{t_{slu}}{t_{slv}} \quad (3)$$

$$\eta_{sp} = \eta_{rel} - 1 \quad (4)$$

Where t_{slv} and t_{slu} are average efflux time of water and aqueous solution of polymer, respectively.

Density

The density of the film samples was determined in triplicate using a pycnometric method with n-hexane as the displacement solvent. The procedure was conducted at a constant ambient temperature of 20 °C. A clean, dry pycnometer was first weighed to obtain its tare mass (W_p). Several pieces of the film were then introduced into the pycnometer, and the combined mass was recorded (W_{ps}). The pycnometer containing the film was subsequently filled with n-hexane, ensuring complete immersion of the samples, and weighed again (W_{psh}). Following this, the clean, dry pycnometer was filled solely with n-hexane and weighed (W_{ph}). Finally, the pycnometer was filled with DW and weighed (W_{pw}) to allow for calibration, given the known density of DW (0.9982 g/cm³ at 20 °C). The densities of n-hexane (D_h) and the film samples (D_s) were subsequently calculated using Eqs. (5) through (7).

$$D_h = \frac{(w_{ph} - w_p)}{(w_{pw} - w_p)/D_w} \quad (5)$$

$$V_s = \frac{(w_{ph} - w_p) - (w_{psh} - w_{ps})}{D_h} \quad (6)$$

$$D_s = \frac{(w_{ps} - w_p)}{V_s} \quad (7)$$

Thickness

The thickness of the films was measured by a routine micrometer with an accuracy of 0.01 mm at 10 random points (Salarbashi et al., 2017).

Moisture Content

To determine the moisture content (MC), film samples were dried in a laboratory oven (Pars Azma Co., Iran) at a constant temperature of 105 ± 1 °C. The mass loss was measured, and the moisture content was subsequently calculated in triplicate using Eq. (8).

$$\text{MC}\ (\%) = \frac{(m_1 - m_2)}{m_1} \times 100 \quad (8)$$

The initial weight of the specimen was recorded as m_1, while the weight of the specimen following oven drying was recorded as m_2.

Film Solubility in Water

Water solubility (SW) was measured in triplicate and defined as the percentage of water-soluble dry matter lost from the initial dry weight of the film. Briefly, 2 cm × 2 cm sections of each film were prepared and dried at 105°C until a constant mass (m_3) was achieved. Subsequently, the dried samples were immersed in 50 mL of DW and agitated gently for 6 h at a controlled temperature of 25°C (Hassannia-Kolaee, Khodaiyan, Pourahmad, & Shahabi-Ghahfarrokhi, 2016). Following immersion, the films were dried again at 105 ± 1°C until a constant weight (m_4) was achieved. The SW of each specimen was determined in triplicate using Eq (9).

$$SW(\%) = \frac{(m_3 - m_4)}{m_4} \times 100 \quad (9)$$

Moisture Absorption

The moisture absorption (MA) properties of the films were determined gravimetrically according to a standard protocol (Goudarzi *et al*., 2017). Film samples (2 cm × 2 cm) were first desiccated over calcium chloride (0% RH) until a constant initial mass (m_5) was achieved. Subsequently, the samples were equilibrated in a desiccator containing a saturated magnesium nitrate solution, maintaining a RH of 50–55%, until a constant final mass (m_6) was attained. The experiment was conducted in triplicate. MA was then calculated using Eq. (10), based on the mass difference before and after conditioning (Goudarzi et al., 2017).

$$\text{MA}\ (\%) = \frac{(m_6 - m_5)}{m_5} \times 100 \quad (10)$$

Contact Angle

Surface wettability is characterized by static water contact angle measurements, determined by the sessile drop method. In this procedure, a 5 µl droplet of distilled water was dispensed onto the sample surface. A profile image of the droplet was then acquired with a digital microscope (AM2111, Dino-Lite, Taiwan) employing backlight illumination to ensure high contrast. The contact angle was then calculated using the CA plugin in ImageJ software (version Java 1.8.0_172) (Goudarzi & Shahabi-Ghahfarrokhi, 2018a). This was performed in triplicate.

Water vapor permeability

The water vapor permeability (WVP) of the films was evaluated in triplicate using the container weight change method, following the ASTM E96-95 standard (Standard, 1989). Glass vials, fabricated to precise specifications (13 mm internal diameter × 45 mm height), were prepared as permeation cells. Each vial contained a charge of calcium chloride desiccant to maintain a 0% RH environment within the internal headspace. Film specimens were mounted hermetically over the mouth of each vial using a double-sided adhesive tape. The prepared assemblies were then equilibrated in a controlled-humidity desiccator, which contained a saturated sodium chloride solution to maintain a constant 75% RH atmosphere. The mass of each vial assembly was monitored gravimetrically to track water vapor permeation. Measurements were recorded periodically using an analytical balance with a precision of ±0.0001 g. Data acquisition was performed at hourly intervals for the initial 8-hour period and continued thereafter until a steady-state mass gain was observed, indicating the attainment of diffusion equilibrium. The steady-state water vapor flux was determined from the linear portion of the mass gain versus time plot, where the slope (S) was calculated by linear regression analysis. The water vapor transmission rate (WVTR) and the WVP were then derived from this slope using Equations (11) and (12), respectively.

$$\mathrm{WVTR} = \frac{S}{A} \quad (11)$$

$$\mathrm{WVP} = \frac{\mathrm{WVTR} \times \mathrm{X}}{\Delta P} \quad (12)$$

where A denotes the effective film area (m^2), X represents the mean film thickness (m), and ΔP is the vapor pressure differential (1753.55 Pa).

Mechanical Properties

The mechanical properties of the films—specifically tensile strength (TS), elongation at break (EB), and tensile energy to break (TEB)—were evaluated in accordance with ASTM standard method D882-02 (Standard, 2004). Measurements were performed in triplicate using a universal testing machine (STM-5, Santam Co., Iran). Prior to testing, rectangular film specimens (100 mm × 10 mm) were conditioned for at least 48 hours at 50–55% RH within a desiccator charged with a saturated magnesium nitrate solution. For analysis, specimens were mounted in the grips with an initial gauge length of 70 mm and elongated at a constant crosshead speed of 50 mm/min. The resultant data were used to calculate the mechanical properties based on Equations (13) through (15).

$$\mathrm{TS}=\frac{\mathrm{F_{Max}}}{\mathrm{A}_{Min}} \quad (13)$$

$$\mathrm{EB}=\frac{\mathrm{L_{Max}}}{\mathrm{L_0}}\times 100 \quad (14)$$

$$\mathrm{TEB}=\mathrm{A_{Stress-Strain}} \quad (15)$$

Where F_{max} is the maximum load (N), A_{min} is the minimum original cross-sectional area (mm^2), L_{max} is the elongation at fracture (mm), L_o is the initial gauge length (mm), and $A_{Stress-Strain}$ is the area beneath the engineering stress-strain curve (MPa), representing the material's toughness.

Color

The color properties of the film samples were analyzed using a portable colorimeter (TES 135A, Electronic CORP, Taiwan) in triplicate. The film specimens were placed on a white standard plate, which provided the calibration background (L* = 96.93, a* = -0.95, b* = 1.86) (Babaei-Ghazvini *et al.*, 2018). From these measurements, the whiteness index (WI) and the total color difference (ΔE) were computed in accordance with Eq. (17) and (16), respectively.

$$\mathrm{WI} = 100 - \sqrt{(100 - L^*)^2 + a^{*2} + b^{*2}} \quad (16)$$

$$\Delta E = \sqrt{(L^* - L)^2 + (a^* - a)^2 + (b^* - b)^2} \quad (17)$$

UV–Vis Spectroscopy

The ultraviolet-visible (UV-Vis) absorption profiles of the nanocomposite films were conducted using a SPECORD 250 UV/VIS spectrophotometer (Analytik Jena, Germany). Spectra were recorded across a wavelength range of 190–800 nm. For analysis, the films were sectioned into 1 × 2 cm^2 segments and mounted in the sample holder against an empty quartz cuvette,

which was used to establish the baseline reference. All measurements were performed in triplicate.

Statistical Analysis

The experimental data, arranged in a completely randomized design, were subjected to a one-way analysis of variance (ANOVA) using SPSS software (v. 23, SPSS Inc., USA). To compare mean values across treatment groups, Duncan's multiple range test was applied, with statistical significance established at the $p < 0.05$ level.

Results and Discussion

Microstructure

The microstructure of the film specimens was investigated using FE-SEM. Fig. 2 and Fig. 3 show microstructure of the surface and the cross-section of SZ and cold plasma-irradiated starch/ZnO (CPSZs) at different exposure times of 30 s, 60 s, and 90 s. The surface of the SZ films is almost uniform with homogenous distribution of ZnO NPs on it, while the ZnO NPs spots were not clear in the cross-section of the SZ films. On the other hand, the etched surfaces by CP have made the rougher surface on the CPSZs compared to the SZ film and created some cavities and fine particles on them. The etching effect on the starch solution was caused by the bombardment of energetic CP species. These species include electrons, ions, radicals, and UV radiation. The interaction of these energetic CP components with the starch solution led to an etching or eroding effect on the starch (Chen *et al.*, 2020; S.K. Pankaj *et al.*, 2015). The roughness of the CPSZs films is drastically higher than the virgin SZ film which agrees with previous studies (Bastos, Santos, da Silva, & Simão, 2009; Heidemann *et al.*, 2019). Although the formation of etching on biopolymeric films in the solid state has been reported (Chen *et al.*, 2020; S.K. Pankaj *et al.*, 2015), the formation of etching in the liquid state is confusing. We also observed this phenomenon in our previous report (Bayanloo, Shahabi-Ghahfarrokhi, & Hagh Nazari, 2024). It seems that CP created a new structure in the matrix of the bionanocomposite. The new structure is a long chain (Table 1-Intrinsic viscosity) with low density (Table 1-Density) and appropriate affinity with the matrix of the bio-nanocomposite (Fig. 2 and Fig. 3). On the other hand, the new SZ structure was broken down to a finer structure with increasing plasma processing times, which is clearly visible in Fig. 3.

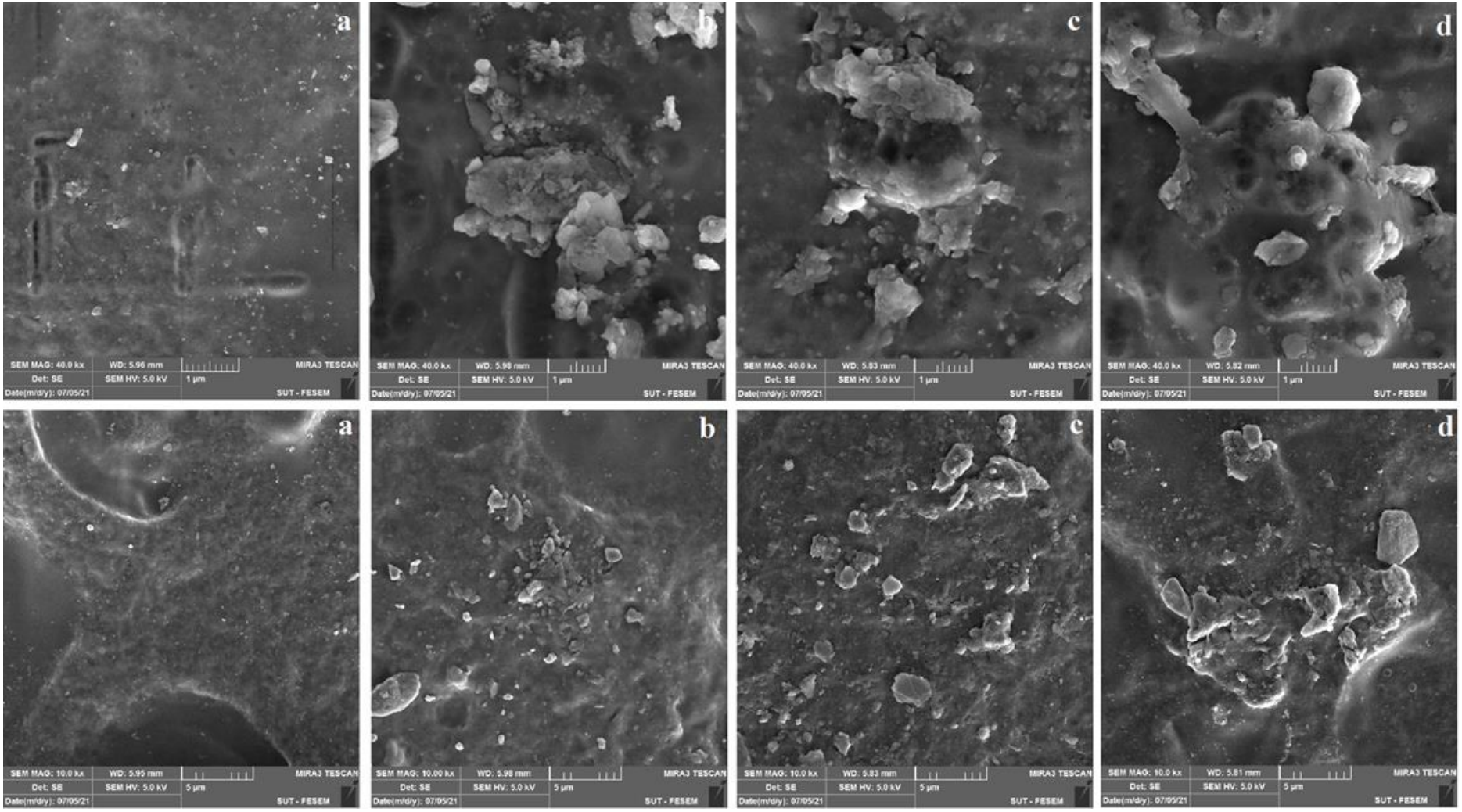

Fig. 2. The surface microstructure of starch/ZnO NPs (SZ) (a) and modified SZ treated with cold plasma at varying exposure times of 30 s (b), 60 s (c), and 90 s (d), shown at different magnifications

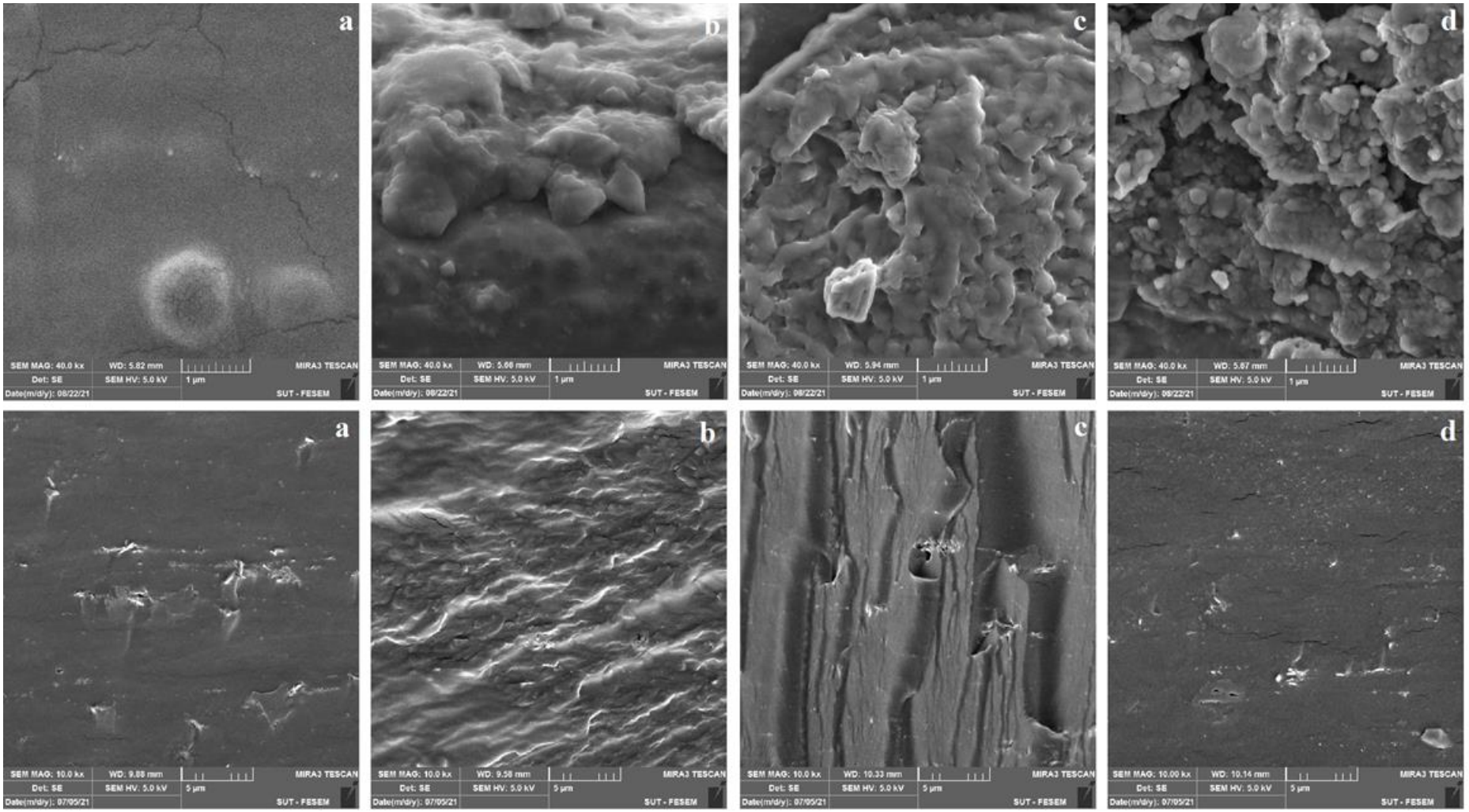

Fig. 3. The cross-sectional microstructure of starch/ZnO NPs (SZ) (a) and modified SZ subjected to CP at exposure times of 30 s (b), 60 s (c), and 90 s (d), depicted at different magnifications.

Intrinsic Viscosity

The intrinsic viscosity of a polymer is influenced by factors such as its average molecular weight, molecular rigidity (determined by bond types and quantity), and molecular configuration (e.g., random coil or rod-like structures) (Momeni *et al.*, 2018). These changes offer valuable information regarding the molecular size and structural characteristics of the polymer.

As shown in Table 1, the intrinsic viscosity of the film-forming solutions increased significantly with longer plasma treatment times. This suggests that reactive plasma species facilitated the formation of a higher molecular weight polymer network in the CPSZs solutions compared to the untreated SZ control. These results align with previous studies demonstrating that the rheological modifications imparted by CP on biopolymers are contingent upon factors including the biopolymer's origin, the plasma generator design, and the working gas composition (Momeni *et al.*, 2018; Shahabi-Ghahfarrokhi, Khodaiyan, Mousavi, & Yousefi, 2015a; Sheikhi *et al.*, 2021). However, they contradict our previous studies, which employed UV (Goudarzi & Shahabi-Ghahfarrokhi, 2018a, 2018b; Shahabi-Ghahfarrokhi & Babaei-Ghazvini, 2019; Shahabi-Ghahfarrokhi *et al.*, 2019) and gamma ray (Shahabi-Ghahfarrokhi *et al.*, 2015a) methods for biopolymer modification. Unlike the UV and gamma ray approaches, which reduced the molecular weight of the biopolymers, the current study using CP resulted in an increase in molecular weight.

Density

Polymer density is a function of multiple critical parameters. These include the molecular weight of the constituent chains, the material's crystallinity, the packing efficiency of the polymer segments, and the properties of incorporated particles, such as their size, distribution, and morphological shape (Bulbul, Bhushette, Zambare, Deshmukh, & Annapure, 2019). A reduction in the density of biopolymers is often associated with an increase in free volume or voids within their structural framework (Mohammadi-Alamuti, Shahabi-Ghahfarrokhi, & Shaterian, 2023). The densities of SZ and CPSZs are presented in Table 1., no significant difference was observed between samples. Previous studies have shown that the density of CP-modified starch and xanthan-based films decreased with longer processing times, up to 20 min. This effect was observed across treatments applied at two different power levels (50 W and 60 W) (Bulbul *et al.*, 2019; Honarvar *et al.*, 2017). It appears that the high density of ZnO NPs counteracted the density reduction observed in modified starch through CP treatment.

Contact Angle

The CA between a water droplet and a film surface serves as an indicator of surface wettability (Honarvar *et al.*, 2017). The Wenzel model is commonly applied to describe CA behavior on rough surfaces with chemical homogeneity (Wenzel, 1936). According to this model, surface roughness intensifies the intrinsic hydrophilic or hydrophobic characteristics of the surface. Specifically, roughness can enhance either wetting or non-wetting behavior, depending on the surface's chemical properties (Cassie & Baxter, 1944; Seo & Kim, 2015).

The CA values for water droplets on the film surfaces are presented in Table 1. A significant reduction in CA was observed for SZ films as the plasma processing times increased. In line with the Wenzel model, the development of a rough surface (Fig. 2) and the modification of the surface chemical structure of SZ through CP treatment contributed to this phenomenon. CP treatment typically results in a notable increase in surface free energy, primarily due to the introduction of polar functional groups on the polymer surface (Pankaj & Thomas, 2016). Additionally, CP generated in an air atmosphere is particularly effective in reducing CA, as the radicals formed on the polymer surface react rapidly with oxygen-containing species in the air (De Geyter, Morent, Leys, Gengembre, & Payen, 2007). These observations align with prior studies

investigating the impact of CP treatment on polymer surface wettability (Bayanloo *et al.*, 2024; Ulbin-Figlewicz, Zimoch-Korzycka, & Jarmoluk, 2014; Wiącek, Jurak, Gozdecka, & Worzakowska, 2017).

Thickness

Film thickness is an essential parameter when calculating the mechanical properties and WVP of films. The thickness of a film is dependent on the preparation methods used to make the film, the drying conditions applied during the film formation process, (Hosseini, Rezaei, Zandi, & Farahmandghavi, 2015)and biopolymers type. Table 1 shows the thickness of the SZ nanocomposite before and after CP irradiation. The thickness of the films was significantly increased by plasma processing times. As shown in Fig. 3, a porous structure was formed by CP in SZ nanocomposites, lead to extension of the thickness of the CPSZs. This change was also observed in previous studies (Li *et al.*, 2011; Wu *et al.*, 2020).

Moisture Content

Table 1 presents the MC values for SZ and CPSZs. The MC of the films decreased after undergoing CP treatment. This reduction in MC was found to be independent of plasma processing times. MC is a parameter that indicates the total void volume occupied by water molecules in the microstructure of biopolymers (Li *et al.*, 2011). However, it appears that the porous structure formed in CPSZs facilitates the escape of moisture during the drying process of the films. This observation aligns with the formation of a porous microstructure (Fig. 3) and the decrease in CA as indicated in Table 1, which was also observed in previous studies (Moosavi *et al.*, 2020; Moradi *et al.*, 2020).

Solubility in Water

The SW is a critical factor influencing the suitability of films for packaging applications, as these films often serve as protective layers for food products (Moosavi *et al.*, 2020). Table 1 presents the SW values for SZ and CPSZs films. The SW of CPSZs films exhibited an increase compared to SZ films, a trend that was independent of plasma processing times. This change can be attributed to the formation of particles through CP etching and the development of a porous microstructure (Fig. 2 and Fig. 3), which enhanced the affinity between water and the biopolymer. This observation is consistent with the changes in CA (Table 1) observed with increasing plasma processing times. The formation of hydrophilic groups on the film surface likely contributed to the increased SW of the biopolymers. Factors such as nanoparticle content, nanoparticle type, biopolymer type, and the gas used for CP generation appear to influence the water sensitivity of bionanocomposites. Furthermore, the ratio of crystalline to amorphous structures disrupted by CP treatment plays a significant role in modifying the moisture sensitivity of biopolymers, as supported by previous studies (Sheikhi *et al.*, 2021).

Moisture Absorption

The water resistance properties of packaging materials are critical in influencing the shelf life of food products (Dong *et al.*, 2018). Consequently, numerous studies have investigated the MA of biopolymers, with a primary focus on improving water resistance (Goudarzi & Shahabi-Ghahfarrokhi, 2018a; Goudarzi *et al.*, 2017; Hassannia-Kolaee, Khodaiyan, Pourahmad, *et al.*, 2016; Hassannia-Kolaee, Khodaiyan, & Shahabi-Ghahfarrokhi, 2016; Shahabi-Ghahfarrokhi *et al.*, 2015a). Table 1 presents the MA values for SZ and CPSZs films. The MA of the films increased following CP treatment, though no significant differences were observed across varying plasma processing times. The hydrophilicity of the films is largely determined by surface morphology, surface chemical composition (including the presence of polar groups), and surface free energy (S. Pankaj *et al.*, 2015). Hence, these polar groups make the surfaces of plasma–treated polymer more hydrophilic compared to the virgin polymer surface (Yang, Chen, Guo, & Zhang, 2009). It appears that the formation of polar groups through CP and the

porous microstructure of CPSZs (Fig. 2 and Fig. 3) contribute to this change. This interpretation is supported by the corresponding CA results, which is in agreement with previous studies (Bayanloo *et al.*, 2024).

Water Vapor Permeability

Starch-based films are hydrophilic, leading to high WVP due to water clustering and diffusion through micro-cavities. This high WVP, driven by vapor pressure differences and the film's inherent structure, is a major limitation for commercial applications like food packaging. Effective packaging requires films that act as barriers to humidity exchange, a property measured directly by WVP testing (Bayanloo *et al.*, 2024; S.K. Pankaj *et al.*, 2015; Romani *et al.*, 2019).

Table 1 shows WVP of the SZ and CPSZs. There was no significant difference between the WVP of SZ and CPSZ. It was anticipated that the porosity, roughness of the surface and cross-section (as depicted in Fig. 2 and Fig. 3), and the formation of polar groups on the biopolymer surface through CP treatment (Table 1-CA) would lead to an increase in WVP. The use of ZnO NPs seems to fill voids and pores within the biopolymer matrix, and create an indirect path for water molecules to pass through. Consequently, the effects of porosity and roughness are nullified. Similar trends have been reported in prior studies (S.K. Pankaj *et al.*, 2015).

Table 1- Physical characteristics of starch/ZnO NPs (SZ) and cold plasma-treated SZ films at varying plasma processing durations (30, 60, and 90 s) ‡, *

Time (s)	Thickness (mm)	Moisture Content (%)	Moisture absorption (%)	Solubility in water (%)	WVP ($\times 10^{-10}$ g m^{-1} s^{-1} Pa^{-1})	Density (g/cm^3)	Contact angle (degree)	Intrinsic viscosity (dl/g)
0	0.14±0.01d	20.83±0.19a	7.30±0.41b	16.01±0.16b	3.24±0.01a	1.42±0.16a	90.39±0.50a	0.12±0.01c
30	0.15±0.02c	20.51±0.11ab	8.43±0.07a	16.36±0.29ab	3.27±0.02a	1.24±0.03a	87.59±0.75b	0.13±0.01bc
60	0.16±0.01b	20.47±0.15b	8.63±0.13a	16.46±0.18a	3.35±0.01a	1.23±0.23a	85.22±0.57c	0.14±0.01ab
90	0.17±0.01a	20.33±0.22b	8.86±0.16a	16.70±0.26a	3.43±0.03a	1.21±0.13a	83.24±0.90d	0.15±0.01a

‡ Values in the same column sharing identical letters indicate no significant difference ($P<0.05$)

* Data are presented as means ± SD

Mechanical Properties

The mechanical properties of biopolymers, specifically strength and flexibility, are critical for preventing structural failure and maintaining product integrity (Ghanbarzadeh & Oromiehi, 2009). These properties were evaluated by measuring TS (the maximum stress before fracture), EB (a measure of flexibility), and TEB (toughness or the total energy absorbed per unit volume before rupture, representing overall durability) (Mohammadi-Alamuti *et al.*, 2023).

The mechanical properties of SZ and CPSZs films are detailed in Table 2. The observed enhancement in these properties can be linked to alterations in molecular weight, rigidity, and/or molecular configuration induced by CP modification, as evidenced by intrinsic viscosity measurements provided in Table 1. It is plausible that the generation of free radicals during CP treatment promotes the formation of cross-links within the film structure. Consequently, the mechanical properties of the film are significantly affected by the quantity and nature of these cross-links, as well as the presence of mono- and disaccharides produced during irradiation, which further modulate these properties. Prior research has also confirmed the efficacy of CP in altering the mechanical characteristics of films (Bayanloo *et al.*, 2024; Moosavi *et al.*, 2020).

Table 2- Mechanical characteristics of starch/ZnO NPs (SZ) films and cold plasma-treated SZ films at varying plasma exposure durations (30, 60, and 90 s)

Time (s)	Tensile strength (MPa)	Elongation at break (%)	Tensile energy to break (MJ/m^3)
0	4.54 ± 0.30 c	41.09 ± 5.63 c	1.54 ± 0.29 c
30	4.92 ± 0.20 bc	47.95 ± 7.19 bc	1.97 ± 0.25 bc
60	5.41 ± 0.30 ab	55.89 ± 0.52 ab	2.33 ± 0.31 ab
90	5.85 ± 0.28 a	59.75 ± 5.10 a	2.72 ± 0.35 a

‡ Values in the same column sharing identical letters indicate no significant difference (P<0.05)
* Data are presented as means ± SD

Color

As shown in Fig. 4, the SZ films demonstrated a transparent appearance. The addition of CP to form CPSZs films did not compromise this visual transparency. Quantitative support for these visual characteristics is provided by the colorimetric data (L^*, a^*, b^*, ΔE, and WI) detailed in Table 3 for both film types. The results indicate that CP significantly influences certain visual properties of CPSZs films, specifically L^*, ΔE, and WI, whereas the parameters a and b remain unaffected. Notably, increasing the plasma processing times led to a reduction in L and WI values, while ΔE values showed a corresponding increase. These findings highlight the impact of CP irradiation on the optical properties of the films.

The development of color in the food packaging materials was likely due to the Maillard reaction occurring between the available carbohydrates and the residual protein (present in the starch). Previous studies have also observed similar color changes in their findings (Bayanloo *et al.*, 2024; Romani *et al.*, 2019).

Table 3- Color parameters (*L*, a*, b), color difference (ΔE), and whiteness index (WI) of starch/ZnO NPs (SZ) and cold plasma-irradiated SZ films, measured at varying plasma processing times of 30, 60, and 90 s**

Time (s)	*L**	*a**	*b**	ΔE	WI
0	92.69 ± 0.30a	-0.67 ± 0.18a	-1.83 ± 0.19a	5.63 ± 0.28c	92.42 ± 0.29a
30	92.33 ± 0.29b	-0.86 ± 0.19a	-1.79 ± 0.01a	5.87 ± 0.22bc	92.08 ± 0.30b
60	91.99 ± 0.43c	-0.90 ± 0.35a	-1.73 ± 0.36a	6.13 ± 0.26ab	91.74 ± 0.40c
90	91.60 ± 0.41d	-0.91 ± 0.18a	-1.67 ± 0.17a	6.39 ± 0.39a	91.38 ± 0.41d

‡ Values in the same column sharing identical letters indicate no significant difference (P<0.05)
* Data are presented as means ± SD

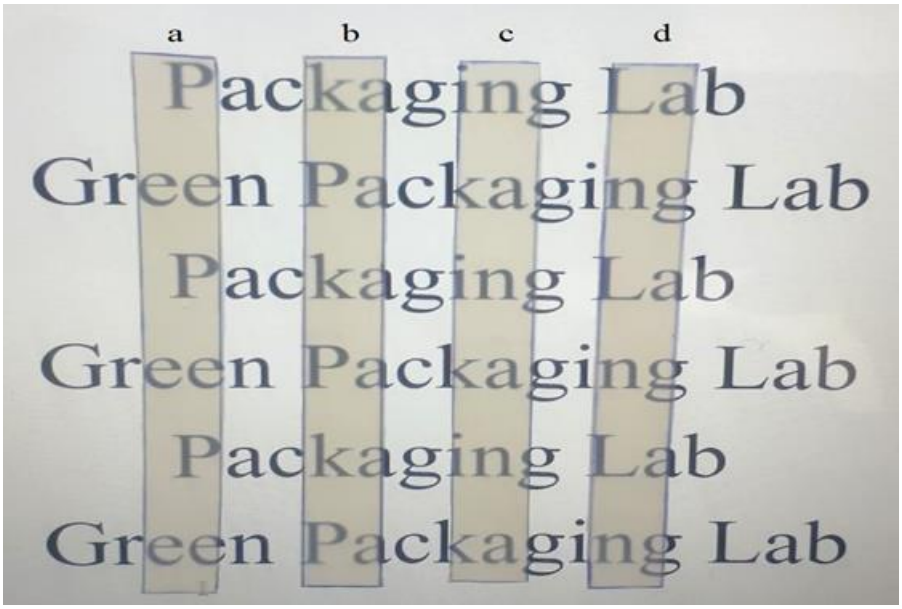

Fig.4. The visual properties of starch/ZnO NPs (SZ) (a) and cold plasma-irradiated SZ films treated at different plasma processing times of 30 s (b), 60 s (c), and 90 s (d).

UV-Vis Spectroscopy

The transmission of UV and visible light through the packaging materials is an important characteristic that can influence the aesthetic appeal of the package and protect the packaged contents from photochemical degradation. This factor can sometimes be more critical than the oxygen permeability of the packaging (Mohammadi-Alamuti *et al.*, 2023). Exposure to UV rays speeds up food spoilage by causing the formation of free radicals, destroying antioxidants, oxidizing lipids, degrading nutrients, and leading to discoloration and off-flavors (Mohammadi-Alamuti *et al.*, 2023). The opacity of the film influences how much light can pass through it, which can be essential for regulating light exposure in certain products (Romani *et al.*, 2020). The efficacy of ZnO as a UV-blocking agent is attributed to its strong absorption of ultraviolet radiation (Babaei-Ghazvini *et al.*, 2018; Shahabi-Ghahfarrokhi & Babaei-Ghazvini, 2019). The incorporation of ZnO into biopolymer packaging compositions can provide protection against photo-oxidation. The UV-Vis spectra of SZ and CPSZs are illustrated in Fig. 5. The CPSZs-90s sample exhibited the highest absorbance among the tested spectra, albeit without statistical significance. This spectral behavior aligns with the visible characteristics of the SZ and CPSZs films presented in Fig 4. The observed effect is consistent with previous research demonstrating that UV irradiation is an effective modification technique for altering

the UV-Vis spectral properties of starch-based films (Babaei-Ghazvini *et al.*, 2018; Shahabi-Ghahfarrokhi & Babaei-Ghazvini, 2019; Shahabi-Ghahfarrokhi *et al.*, 2019). It appears that the wavelength, intensity, and exposure time of the applied UV rays significantly affect the transparency of the modified SZ films.

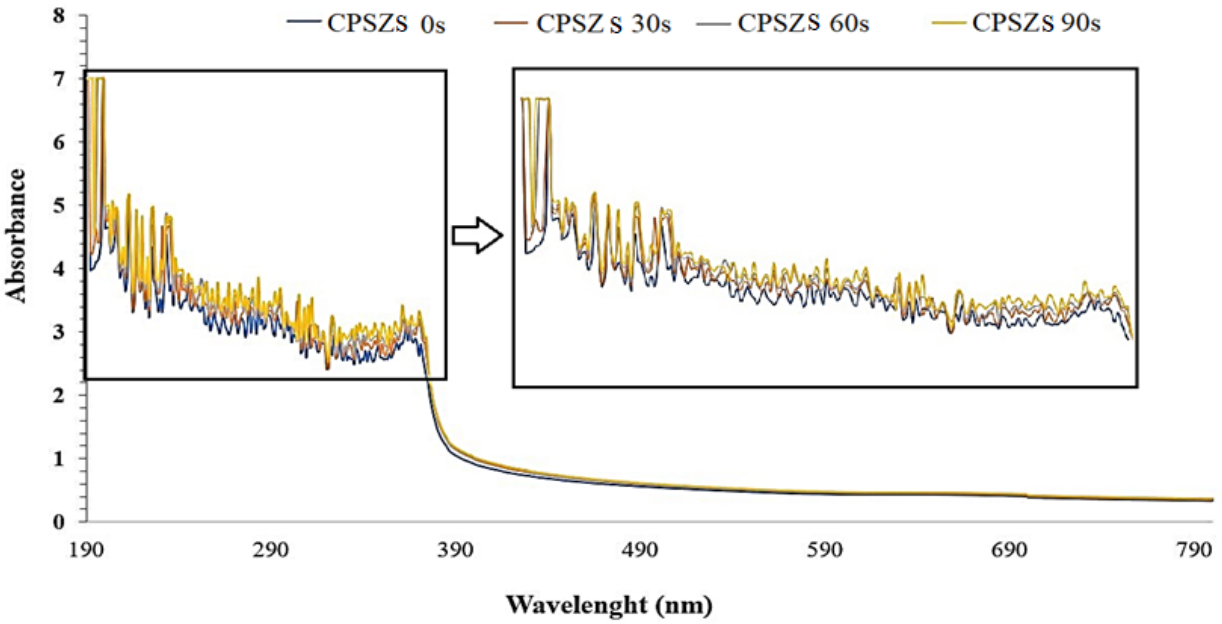

Fig. 5. The UV-Vis absorption spectra of starch/ZnO NPs (SZ) and cold plasma-irradiated SZ films processed at different exposure times of 30 s (CPSZs 30s), 60 s (CPSZs 60s), and 90 s (CPSZs 90s).

Conclusion

Despite the impressive properties of petroleum-based plastics in food packaging, there is growing concern over their environmental impact. As a result, starch-based packaging materials have gained attention as potential substitutes for plastics. In the current study, two modification methods (i.e., nano reinforcement and CP) were employed to address the limitations of starch-based packaging materials.

Previous studies have utilized CP to modify biopolymers, but it has been a time-consuming process, making it impractical for the packaging industry. However, in this study, simultaneous CP in an aqueous solution with the addition of ZnO was found to effectively modify the packaging properties of starch in a shorter time (e.g., 30 to 90 seconds). The high moisture content of the film-forming solution and the presence of photo-active nanoparticles (i.e., ZnO) were found to intensify the formation of reactive plasma species (e.g., free radicals, ions, electrons). As a result, the modification of starch-based nanocomposites was accelerated in the current study compared to previous studies.

The application of CP was observed to improve the mechanical properties (e.g., TS, EB, TEB) of SZ films without negatively affecting their visual characteristics. However, no significant alterations were noted in the UV-blocking capabilities of the SZ films. While CP did not substantially influence the water sensitivity of SZ films, it increased the hydrophilicity of the film surface. This effect can be linked to the formation of polar groups and the development of a rougher surface texture due to etching in CPSZs films. The uniform dispersion of ZnO achieved through CP was identified as a critical factor contributing to the enhanced packaging properties of CPSZs films.

Based on the bibliography and the results of this study, it is evident that the simultaneous application of CP and SZ is beneficial for coating and surface pasteurization of food products such as nuts, meats, and fruits.

Subsequent investigations should examine the application of CP with alternative gases for starch modification. Concurrently, research must quantify the active species produced during plasma treatment and assess the impact of any residual compounds on the sensory and physicochemical properties of the treated food products.

Author Contributions

Amir-Hossein Bayanloo: methodology, validation, formal analysis, investigation, writing—original draft preparation, and visualization. **Iman Shahabi-Ghahfarrokhi**: conceptualization, methodology, validation, formal analysis, writing—review and editing, supervision, funding acquisition, and project administration. **Simin Hagh-Nazari**: methodology, validation, formal analysis, and supervision.

Funding and Thesis Origin

This article is derived from a Master's thesis registered under tracking code 1626888 in the IranDoc database. The research was financially supported by the University of Zanjan.

References

1. Ali, H., & Ghaffar, A.A. (2017). Preparation and effect of gamma radiation on the properties and biodegradability of poly (styrene/starch) blends. *Radiation Physics and Chemistry, 130*, 411-420. https://doi.org/10.1016/j.radphyschem.2016.09.006
2. Almasi, H., Ghanbarzadeh, B., & Entezami, A.A. (2010). Physicochemical properties of starch–CMC–nanoclay biodegradable films. *International Journal of Biological Macromolecules, 46*(1), 1-5. https://doi.org/10.1016/j.ijbiomac.2009.10.001
3. Babaei-Ghazvini, A., Shahabi-Ghahfarrokhi, I., & Goudarzi, V. (2018). Preparation of UV-protective starch/kefiran/ZnO nanocomposite as a packaging film: Characterization. *Food Packaging and Shelf Life, 16*, 103-111. https://doi.org/10.1016/j.fpsl.2018.01.008
4. Bastos, D.C., Santos, A.E., da Silva, M.L., & Simão, R.A. (2009). Hydrophobic corn starch thermoplastic films produced by plasma treatment. *Ultramicroscopy, 109*(8), 1089-1093. https://doi.org/10.1016/j.ultramic.2009.03.031
5. Bayanloo, A.H., Shahabi-Ghahfarrokhi, I., & Hagh Nazari, S. (2024). Modification and characterization of starch-based food-packaging material by cold plasma as a green approach. *Starch-Stärke, 76*(5-6), 2300077. https://doi.org/10.1002/star.202300077
6. Bulbul, V., Bhushette, P.R., Zambare, R.S., Deshmukh, R., & Annapure, U.S. (2019). Effect of cold plasma treatment on Xanthan gum properties. *Polymer Testing, 79*, 106056. https://doi.org/10.1016/j.polymertesting.2019.106056
7. Cassie, A., & Baxter, S. (1944). Wettability of porous surfaces. *Transactions of the Faraday Society, 40*, 546-551. https://doi.org/10.1039/TF9444000546
8. Chen, G., Chen, Y., Jin, N., Li, J., Dong, S., Li, S., & Chen, Y. (2020). Zein films with porous polylactic acid coatings via cold plasma pre-treatment. *Industrial Crops and Products, 150*, 112382. https://doi.org/10.1016/j.indcrop.2020.112382
9. Cheng, H., Chen, L., McClements, D.J., Yang, T., Zhang, Z., Ren, F., & Jin, Z. (2021). Starch-based biodegradable packaging materials: A review of their preparation, characterization and diverse applications in the food industry. *Trends in Food Science & Technology, 114*, 70-82. https://doi.org/10.1016/j.tifs.2021.05.017
10. De Geyter, N., Morent, R., Leys, C., Gengembre, L., & Payen, E. (2007). Treatment of polymer films with a dielectric barrier discharge in air, helium and argon at medium pressure. *Surface and Coatings Technology, 201*(16-17), 7066-7075. https://doi.org/10.1016/j.surfcoat.2007.01.008

11. Dimitrakellis, P., & Gogolides, E. (2018). Hydrophobic and superhydrophobic surfaces fabricated using atmospheric pressure cold plasma technology: A review. *Advances in Colloid and Interface Science, 254*, 1-21. https://doi.org/10.1016/j.cis.2018.03.009
12. Dong, S., Guo, P., Chen, Y., Chen, G.-y., Ji, H., Ran, Y., & Chen, Y. (2018). Surface modification via atmospheric cold plasma (ACP): Improved functional properties and characterization of zein film. *Industrial Crops and Products, 115*, 124-133. https://doi.org/10.1016/j.indcrop.2018.01.080
13. El Fawal, G., Hong, H., Song, X., Wu, J., Sun, M., He, C., & Wang, H. (2020). Fabrication of antimicrobial films based on hydroxyethylcellulose and ZnO for food packaging application. *Food Packaging and Shelf Life, 23*, 100462. https://doi.org/10.1016/j.fpsl.2020.100462
14. Ghanbarzadeh, B., & Oromiehi, A. (2009). Thermal and mechanical behavior of laminated protein films. *Journal of Food Engineering, 90*(4), 517-524. https://doi.org/10.1016/j.jfoodeng.2008.07.018
15. Ghasemlou, M., Khodaiyan, F., Jahanbin, K., Gharibzahedi, S.M.T., & Taheri, S. (2012). Structural investigation and response surface optimisation for improvement of kefiran production yield from a low-cost culture medium. *Food Chemistry, 133*(2), 383-389. https://doi.org/10.1016/j.foodchem.2012.01.046
16. Goiana, M.L., de Brito, E.S., Alves Filho, E.G., de Castro Miguel, E., Fernandes, F.A.N., de Azeredo, H.M.C., & de Freitas Rosa, M. (2021). Corn starch based films treated by dielectric barrier discharge plasma. *International Journal of Biological Macromolecules, 183*, 2009-2016. https://doi.org/10.1016/j.ijbiomac.2021.05.210
17. Goudarzi, V., & Shahabi-Ghahfarrokhi, I. (2018a). Development of photo-modified starch/kefiran/TiO_2 bio-nanocomposite as an environmentally-friendly food packaging material. *International Journal of Biological Macromolecules, 116*, 1082-1088. https://doi.org/10.1016/j.ijbiomac.2018.05.138
18. Goudarzi, V., & Shahabi-Ghahfarrokhi, I. (2018b). Photo-producible and photo-degradable starch/TiO_2 bionanocomposite as a food packaging material: Development and characterization. *International Journal of Biological Macromolecules, 106*, 661-669. https://doi.org/10.1016/j.ijbiomac.2017.08.058
19. Goudarzi, V., Shahabi-Ghahfarrokhi, I., & Babaei-Ghazvini, A. (2017). Preparation of ecofriendly UV-protective food packaging material by starch/TiO_2 bio-nanocomposite: Characterization. *International Journal of Biological Macromolecules, 95*, 306-313. https://doi.org/10.1016/j.ijbiomac.2016.11.065
20. Hassannia-Kolaee, M., Khodaiyan, F., Pourahmad, R., & Shahabi-Ghahfarrokhi, I. (2016). Development of ecofriendly bionanocomposite: Whey protein isolate/pullulan films with nano-SiO_2. *International Journal of Biological Macromolecules, 86*, 139-144. https://doi.org/10.1016/j.ijbiomac.2016.01.032
21. Hassannia-Kolaee, M., Khodaiyan, F., & Shahabi-Ghahfarrokhi, I. (2016). Modification of functional properties of pullulan–whey protein bionanocomposite films with nanoclay. *Journal of Food Science and Technology, 53*(2), 1294-1302. https://doi.org/10.1007/s13197-015-1778-3
22. Heidemann, H.M., Dotto, M.E., Laurindo, J.B., Carciofi, B.A., & Costa, C. (2019). Cold plasma treatment to improve the adhesion of cassava starch films onto PCL and PLA surface. *Colloids and Surfaces A: Physicochemical and Engineering Aspects, 580*, 123739. https://doi.org/10.1016/j.colsurfa.2019.123739
23. Honarvar, Z., Farhoodi, M., Khani, M.R., Mohammadi, A., Shokri, B., Ferdowsi, R., & Shojaee-Aliabadi, S. (2017). Application of cold plasma to develop carboxymethyl cellulose-coated polypropylene films containing essential oil. *Carbohydrate Polymers, 176*, 1-10. https://doi.org/10.1016/j.carbpol.2017.08.054
24. Hosseini, S.F., Rezaei, M., Zandi, M., & Farahmandghavi, F. (2015). Fabrication of bio-nanocomposite films based on fish gelatin reinforced with chitosan nanoparticles. *Food Hydrocolloids, 44*, 172-182. https://doi.org/10.1016/j.foodhyd.2014.09.004

25. Li, Y., Jiang, Y., Liu, F., Ren, F., Zhao, G., & Leng, X. (2011). Fabrication and characterization of TiO_2/whey protein isolate nanocomposite film. *Food Hydrocolloids, 25*(5), 1098-1104. https://doi.org/10.1016/j.foodhyd.2010.10.006
26. Liu, J., Huang, J., Hu, Z., Li, G., Hu, L., Chen, X., & Hu, Y. (2021). Chitosan-based films with antioxidant of bamboo leaves and ZnO nanoparticles for application in active food packaging. *International Journal of Biological Macromolecules, 189*, 363-369. https://doi.org/10.1016/j.ijbiomac.2021.08.136
27. Maniglia, B.C., Castanha, N., Rojas, M.L., & Augusto, P.E. (2021). Emerging technologies to enhance starch performance. *Current Opinion in Food Science, 37*, 26-36. https://doi.org/10.1016/j.cofs.2020.09.003
28. Mohammadi-Alamuti, M., Shahabi-Ghahfarrokhi, I., & Shaterian, M. (2023). Photo–degradable and recyclable starch/Fe_3O_4/TiO_2 nanocomposites: feasibility of an approach to reduce the recycling labor cost in plastic waste management. *Environmental Science and Pollution Research, 30*(2), 2740-2753. https://doi.org/10.1007/s11356-022-22049-1
29. Momeni, M., Tabibiazar, M., Khorram, S., Zakerhamidi, M., Mohammadifar, M., Valizadeh, H., & Ghorbani, M. (2018). Pectin modification assisted by nitrogen glow discharge plasma. *International Journal of Biological Macromolecules, 120*, 2572-2578. https://doi.org/10.1016/j.ijbiomac.2018.09.033
30. Moosavi, M.H., Khani, M.R., Shokri, B., Hosseini, S.M., Shojaee-Aliabadi, S., & Mirmoghtadaie, L. (2020). Modifications of protein-based films using cold plasma. *International Journal of Biological Macromolecules, 142*, 769-777. https://doi.org/10.1016/j.ijbiomac.2019.10.017
31. Moradi, E., Moosavi, M.H., Hosseini, S.M., Mirmoghtadaie, L., Moslehishad, M., Khani, M.R., & Shojaee-Aliabadi, S. (2020). Prolonging shelf life of chicken breast fillets by using plasma-improved chitosan/low density polyethylene bilayer film containing summer savory essential oil. *International Journal of Biological Macromolecules, 156*, 321-328. https://doi.org/10.1016/j.ijbiomac.2020.03.226
32. Pankaj, S., Bueno-Ferrer, C., Misra, N., O'neill, L., Tiwari, B., Bourke, P., & Cullen, P. (2015). Characterization of dielectric barrier discharge atmospheric air cold plasma treated gelatin films. *Food Packaging and Shelf Life, 6*, 61-67. https://doi.org/10.1016/j.fpsl.2015.09.002
33. Pankaj, S., & Thomas, S. (2016). Cold plasma applications in food packaging. In *Cold plasma in food and agriculture* (pp. 293-307): Elsevier. https://doi.org/10.1016/b978-0-12-801365-6.00012-3
34. Pankaj, S.K., Bueno-Ferrer, C., Misra, N., O'Neill, L., Tiwari, B., Bourke, P., & Cullen, P. (2015). Dielectric barrier discharge atmospheric air plasma treatment of high amylose corn starch films. *LWT-Food Science and Technology, 63*(2), 1076-1082. https://doi.org/10.1016/j.lwt.2015.04.027
35. Romani, V.P., Olsen, B., Collares, M.P., Oliveira, J.R.M., Prentice-Hernández, C., & Martins, V.G. (2019). Improvement of fish protein films properties for food packaging through glow discharge plasma application. *Food Hydrocolloids, 87*, 970-976. https://doi.org/10.1016/j.foodhyd.2018.09.022
36. Romani, V.P., Olsen, B., Collares, M.P., Oliveira, J.R.M., Prentice, C., & Martins, V.G. (2020). Cold plasma and carnauba wax as strategies to produce improved bi-layer films for sustainable food packaging. *Food Hydrocolloids, 108*, 106087. https://doi.org/10.1016/j.foodhyd.2020.106087
37. Salarbashi, D., Mortazavi, S.A., Noghabi, M.S., Bazzaz, B.S.F., Sedaghat, N., Ramezani, M., & Shahabi-Ghahfarrokhi, I. (2016). Development of new active packaging film made from a soluble soybean polysaccharide incorporating ZnO nanoparticles. *Carbohydrate Polymers, 140*, 220-227. https://doi.org/10.1016/j.carbpol.2015.12.043
38. Salarbashi, D., Noghabi, M.S., Bazzaz, B.S.F., Shahabi-Ghahfarrokhi, I., Jafari, B., & Ahmadi, R. (2017). Eco-friendly soluble soybean polysaccharide/nanoclay Na+ bionanocomposite: Properties and characterization. *Carbohydrate Polymers, 169*, 524-532. https://doi.org/10.1016/j.carbpol.2017.04.011
39. Seo, K., & Kim, M. (2015). Re-derivation of Young's equation, Wenzel equation, and Cassie-Baxter equation based on energy minimization. In *Surface energy*: IntechOpen. https://doi.org/10.5772/61066

40. Shahabi-Ghahfarrokhi, I., Almasi, H., & Babaei-Ghazvini, A. (2020). Characteristics of biopolymers from natural resources. In *Processing and development of polysaccharide-based biopolymers for packaging applications* (pp. 49-95): Elsevier. https://doi.org/10.1016/b978-0-12-818795-1.00003-4
41. Shahabi-Ghahfarrokhi, I., & Babaei-Ghazvini, A. (2019). Using photo-modification to compatibilize nano-ZnO in development of starch-kefiran-ZnO green nanocomposite as food packaging material. *International Journal of Biological Macromolecules, 124*, 922-930. https://doi.org/10.1016/j.ijbiomac.2018.11.241
42. Shahabi-Ghahfarrokhi, I., Goudarzi, V., & Babaei-Ghazvini, A. (2019). Production of starch based biopolymer by green photochemical reaction at different UV region as a food packaging material: Physicochemical characterization. *International Journal of Biological Macromolecules, 122*, 201-209. https://doi.org/10.1016/j.ijbiomac.2018.10.154
43. Shahabi-Ghahfarrokhi, I., Khodaiyan, F., Mousavi, M., & Yousefi, H. (2015a). Effect of γ-irradiation on the physical and mechanical properties of kefiran biopolymer film. *International Journal of Biological Macromolecules, 74*, 343-350. https://doi.org/10.1016/j.ijbiomac.2014.11.038
44. Shahabi-Ghahfarrokhi, I., Khodaiyan, F., Mousavi, M., & Yousefi, H. (2015b). Preparation of UV-protective kefiran/nano-ZnO nanocomposites: physical and mechanical properties. *International Journal of Biological Macromolecules, 72*, 41-46. https://doi.org/10.1016/j.ijbiomac.2014.07.047
45. Sharma, S. (2020). Cold plasma treatment of dairy proteins in relation to functionality enhancement. *Trends in Food Science & Technology, 102*, 30-36. https://doi.org/10.1016/j.tifs.2020.05.013
46. Sheikhi, Z., Mirmoghtadaie, L., Abdolmaleki, K., Khani, M.R., Farhoodi, M., Moradi, E., & Shojaee-Aliabadi, S. (2021). Characterization of physicochemical and antimicrobial properties of plasma-treated starch/chitosan composite film. *Packaging Technology and Science, 34*(7), 385-392. https://doi.org/10.1002/pts.2559
47. Souza, V.G.L., & Fernando, A.L. (2016). Nanoparticles in food packaging: Biodegradability and potential migration to food—A review. *Food Packaging and Shelf Life, 8*, 63-70. https://doi.org/10.1016/j.fpsl.2016.04.001
48. Standard, A. (1989). Standard test methods for water vapor transmission of materials. In: Annual book of ASTM standards, Designation E96-E80.
49. Standard, A. (2004). Annual book of ASTM standards. *American Society for Testing and Materials Annual, Philadelphia, PA, USA, 4*(04.08).
50. Ulbin-Figlewicz, N., Zimoch-Korzycka, A., & Jarmoluk, A. (2014). Antibacterial activity and physical properties of edible chitosan films exposed to low-pressure plasma. *Food and Bioprocess Technology, 7*(12), 3646-3654. https://doi.org/10.1007/s11947-014-1379-6
51. Venkateshaiah, A., Havlíček, K., Timmins, R.L., Röhrl, M., Wacławek, S., Nguyen, N.H., Agarwal, S. (2021). Alkenyl succinic anhydride modified tree-gum kondagogu: A bio-based material with potential for food packaging. *Carbohydrate Polymers, 266*, 118126. https://doi.org/10.1016/j.carbpol.2021.118126
52. Wenzel, R.N. (1936). Resistance of solid surfaces to wetting by water. *Industrial & Engineering Chemistry, 28*(8), 988-994. https://doi.org/10.1021/ie50320a024
53. Wiącek, A.E., Jurak, M., Gozdecka, A., & Worzakowska, M. (2017). Interfacial properties of PET and PET/starch polymers developed by air plasma processing. *Colloids and Surfaces A: Physicochemical and Engineering Aspects, 532*, 323-331. https://doi.org/10.1016/j.colsurfa.2017.04.074
54. Wihodo, M., & Moraru, C.I. (2013). Physical and chemical methods used to enhance the structure and mechanical properties of protein films: A review. *Journal of Food Engineering, 114*(3), 292-302. https://doi.org/10.1016/j.jfoodeng.2012.08.021
55. Wu, X., Liu, Q., Luo, Y., Murad, M. S., Zhu, L., & Mu, G. (2020). Improved packing performance and structure-stability of casein edible films by dielectric barrier discharges (DBD) cold plasma. *Food Packaging and Shelf Life, 24*, 100471. https://doi.org/10.1016/j.fpsl.2020.100471
56. Yang, L., Chen, J., Guo, Y., & Zhang, Z. (2009). Surface modification of a biomedical polyethylene terephthalate (PET) by air plasma. *Applied Surface Science, 255*(8), 4446-4451. https://doi.org/10.1016/j.apsusc.2008.11.048

مقاله پژوهشی

جلد ۲۱، شماره ٦، بهمن- اسفند ١٤٠٤، ص.

اثر پلاسما سرد و نانواکسید روی بر اصلاح نشاسته ذرت به‌عنوان ماده بسته‌بندی غذایی

امیرحسین بیانلو[۱]- ایمان شهابی قهفرخی[۱،۲]- سیمین حق نظری[۱]

تاریخ دریافت: ۱۴۰۴/۰۴/۲۶

تاریخ پذیرش: ۱۴۰۴/۰۶/۳۰

چکیده

این پژوهش به بررسی اثر پلاسما سرد بر فیلم‌های بیونانوکامپوزیت دوستدار محیط‌زیست نشاسته/اکسید روی می‌پردازد که شامل ۳ درصد وزنی نانوذره اکسید روی و زمان‌های مختلف اعمال پلاسما سرد (۰، ۳۰، ۶۰ و ۹۰ ثانیه) هستند. نتایج نشان می‌دهد که افزایش مدت زمان تیمار پلاسما سرد موجب افزایش ضخامت فیلم، ویسکوزیته، حلالیت در آب، جذب رطوبت و زبری سطح می‌شود؛ در حالی‌که زاویه تماس و میزان رطوبت کاهش می‌یابد. ولی تغییر قابل توجهی در نفوذپذیری بخار آب، چگالی و یا ارزیابی تراوایی به طیف‌های UV-Vis مشاهده نشد. تیمار پلاسما سرد باعث بهبود استحکام کششی، درصد افزایش طول در نقطه شکست و انرژی کششی تا نقطه شکست در نمونه‌ها شد، در حالی‌که شاخص‌های روشنایی و سفیدی کاهش یافتند بدون آنکه تفاوت رنگی ایجاد شود. این مطالعه پلاسما سرد را به‌عنوان روشی سریع و سازگار با محیط‌زیست برای اصلاح فیلم‌ها معرفی می‌کند که کارایی بیشتری هنگام اعمال بر محلول‌های نشاسته‌ای دارد و پتانسیل بالایی برای کاربردهای صنعتی در مواد بسته‌بندی فراهم می‌آورد.

واژه‌های کلیدی: اصلاح دوگانه، اکسید روی، بسته‌بندی سبز، پلاسما سرد، نانوکامپوزیت، نشاسته

۱- گروه علوم و مهندسی صنایع غذایی، دانشکده کشاورزی، دانشگاه زنجان، زنجان، ایران

۲- گروه علوم و صنایع غذایی، دانشکده کشاورزی، دانشگاه صنعتی اصفهان، اصفهان، ایران

(*- نویسنده مسئول: Email: i.shahabi@znu.ac.ir)

https://doi.org/10.22067/ifstrj.2025.94463.1455